JOURNAL OF AIRCRAFT
Vol. 41, No. 5, September–October 2004

The μ-k Method for Robust Flutter Solutions

Dan Borglund*
Royal Institute of Technology, SE-100 44 Stockholm, Sweden

A straightforward frequency-domain method for robust flutter analysis is presented. First, a versatile uncertainty description for the unsteady aerodynamic forces is derived by assigning uncertainty to the frequency-domain pressure coefficients. The uncertainty description applies to any frequency-domain aerodynamic method, benefits from the same level of geometric detail as the underlying aerodynamic model, exploits the modal formulation of the flutter equation, and is computed by simple postprocessing of standard aerodynamic data. Next, structured singular value analysis is applied to derive an explicit criterion for robust flutter stability based on the flutter equation and a parametric uncertainty description. The resulting procedure for computation of a worst-case flutter boundary resembles a *p-k* or *g*-method flutter analysis, produces match-point flutter solutions and allows for detailed aerodynamic uncertainty descriptions. Finally, the proposed method is successfully applied to a wind-tunnel model in low-speed airflow.

Introduction

In recent years, the structured singular value (or μ) framework from robust control theory has paved the way for robust aeroservoelastic analysis and design.[1–6] Most importantly, this approach allows for a computation of the worst-case flutter speed subject to a specified uncertainty description. If the robust flutter analysis is to be meaningful, it is thus of vital importance to derive an uncertainty description that captures the true uncertainty mechanism both in terms of structure and magnitude. This is typically performed in two steps.[7] In the first step, the uncertainty mechanism is identified and modeled, which settles the structure of the uncertainty. If suitable experimental data are available, the magnitude of the model uncertainty can then be estimated in a second step.

Among the numerous sources of uncertainty in aeroservoelastic models, perhaps is the modeling of unsteady aerodynamic forces the most significant. Previous work has considered uncertainty in finite-state approximations of the aerodynamic forces[1,2] and in frequency-domain lifting-line aerodynamics.[5,6] This paper will present a generalization to frequency-domain aerodynamics in general, which is based on uncertainty in the lifting surface-pressure coefficients. A significant advantage with this approach is that the underlying aerodynamic model can be exploited for development of very detailed uncertainty descriptions. The aerodynamic uncertainty can now be confined to certain regions of the lifting surfaces, allowing for modeling of uncertain external store aerodynamics, control surface aerodynamics, wing-tip aerodynamics and so on. This also means that less significant aerodynamic perturbations can be treated as such, that nonexisting aerodynamic perturbations can be avoided, and that a less conservative worst-case flutter boundary can be computed. The paper includes a case study of a wind-tunnel model in low-speed airflow, where this is clearly indicated.

The method for robust flutter analysis presented in this paper differs somewhat from the μ method developed by Lind and Brenner[1] and Lind.[2] The most essential differences are that the present method is based on the frequency-domain representation of the unsteady aerodynamic forces, rather than a finite-state approximation thereof, and that the flight condition is treated in a traditional manner. As a result, the present method resembles a *p-k* or *g*-method flutter analysis,[8,9] inherently produces match-point flutter solutions, and allows for detailed aerodynamic uncertainty descriptions.

Received 11 June 2003; revision received 24 November 2003; accepted for publication 25 November 2003.

*Research Associate, Department of Aeronautical and Vehicle Engineering, Teknikringen 8. Member AIAA.

Frequency-Domain Flutter Analysis

The Laplace-domain flutter equation can be written in the nondimensional form

$$[\boldsymbol{M}p^2+(L/V)\boldsymbol{D}p+(L^2/V^2)\boldsymbol{K}-(\rho L^2/2)\boldsymbol{Q}(p, M)]\boldsymbol{\eta}(p) = 0 \quad (1)$$

where V is the true airspeed; L is the aerodynamic reference length (usually the reference semichord); ρ is the air density; M is the flight Mach number; $\boldsymbol{\eta}(p)$ is the vector of Laplace-domain generalized coordinates for m elastic modes; $\boldsymbol{M}$, $\boldsymbol{D}$, and $\boldsymbol{K}$ are the $m \times m$ generalized mass, structural modal damping and stiffness matrices, respectively; and $\boldsymbol{Q}(p, M)$ is the $m \times m$ generalized aerodynamic transfer function matrix. The nondimensional Laplace variable p is commonly expressed as $p = g + ik$, where g is the the nondimensional damping, k is the reduced frequency

$$k = \omega L/V \quad (2)$$

and ω is the frequency of vibration.

In the flutter equation (1), the flight condition is said to be match point if the air density ρ, airspeed V, and Mach M are related through an atmospheric model. Incorporating such a model, the flight condition is commonly specified in terms of the dynamic pressure $q = \rho V^2/2$ and Mach M or airspeed V and flight altitude h. Correspondingly, the flutter boundary is typically presented in terms of critical dynamic pressure q vs Mach M or critical airspeed V vs flight altitude h.

For a given flight condition, the flutter equation (1) is a nonlinear eigenvalue problem that defines a set of eigenvalues p and corresponding eigenvectors $\boldsymbol{\eta}$. If q is increased while keeping M fixed, the flutter boundary is reached when some eigenvalue crosses the stability boundary $g = 0$. The most common methods for flutter analysis, such as the *p-k* and *g*-methods,[8,9] compute the flutter boundary in this fashion using approximations of $\boldsymbol{Q}(p, M)$ in the eigenvalue problem Eq. (1). The main reason for this is that most of the unsteady aerodynamic methods used by the aerospace industry only provide the frequency-domain aerodynamic matrix $\boldsymbol{Q}(ik, M)$.[10–13]

The problem posed in this paper is to compute a worst-case flutter boundary when the transfer functions in Eq. (1) are subject to uncertainty. In the next section, particular attention will be given to the problem of modeling uncertainty in the unsteady aerodynamic forces, a matter of fundamental importance in robust flutter analysis.

Uncertainty in Frequency-Domain Aerodynamic Forces

A quite versatile uncertainty description for the unsteady aerodynamic forces can be obtained by considering uncertainty in the

frequency-domain pressure coefficients for a lifting surface. Let $\boldsymbol{Q}_0(ik, M)$ denote the nominal aerodynamic matrix (in the absence of uncertainty) and decompose it according to

$$\boldsymbol{Q}_0(ik, M) = \boldsymbol{R}_0\boldsymbol{S}_0(ik, M) \tag{3}$$

where $\boldsymbol{S}_0(ik, M)$ is the matrix relating the generalized coordinates and the nominal pressure coefficients and $\boldsymbol{R}_0$ is the matrix relating the pressure coefficients and the generalized aerodynamic forces. Note that the results presented in this paper hold for any aerodynamic method that can be used to compute $\boldsymbol{Q}_0(ik, M)$ and that this matrix is part of the data required for a nominal flutter analysis.[8,9]

An aerodynamic uncertainty description emphasizing regions with high pressure loading is obtained by assigning multiplicative uncertainty to the pressure coefficients. If a complex norm-bounded multiplicative uncertainty is assigned to the jth pressure coefficient, the uncertain aerodynamic matrix can be written as

$$\boldsymbol{Q}(ik, M) = \boldsymbol{R}_0(\boldsymbol{I} + w_j\delta_j\boldsymbol{E}_j)\boldsymbol{S}_0(ik, M) = \boldsymbol{Q}_0(ik, M) + w_j\delta_j\boldsymbol{Q}_j(ik, M) \tag{4}$$

where the real weight $w_j \geq 0$ determines the upper bound on the magnitude of the uncertainty, the complex uncertainty parameter δ_j belongs to the set $|\delta_j| \leq 1$, and the matrix $\boldsymbol{E}_j$ has one nonzero element $e_{jj} = 1$. Further, the perturbation matrix

$$\boldsymbol{Q}_j(ik, M) = \boldsymbol{R}_0\boldsymbol{E}_j\boldsymbol{S}_0(ik, M) \tag{5}$$

represents the contribution from the jth pressure coefficient to the generalized aerodynamic forces. For example, if $w_j = 0.1$ the uncertain aerodynamic matrix $\boldsymbol{Q}(ik, M)$ in Eq. (4) defines the set of possible aerodynamic forces when a 10% uncertainty bound is assigned to the jth pressure coefficient. If it is more likely that the uncertainty will tend to increase the load distribution than decrease it, or vice versa, a shifted perturbation can be introduced in order to capture this.[14]

It is reasonable to assume that the aerodynamic uncertainty depends on the flight condition as well as the reduced frequency. If the basic uncertainty mechanism remains the same, this can be accounted for by allowing the uncertainty bound to vary across frequency and/or flight condition. This will mainly result in a more involved procedure for estimation of the uncertainty bound, an issue that will be discussed later on in the paper.

With the present approach, the most general uncertainty description possible is obtained by assigning one uncertain parameter δ_j to each pressure coefficient, giving

$$\boldsymbol{Q}(ik, M) = \boldsymbol{Q}_0(ik, M) + \sum_{j=1}^{n} w_j\delta_j\boldsymbol{Q}_j(ik, M) \tag{6}$$

where n is the total number of pressure coefficients. However, this uncertainty description is not very useful in practice. Even if the true aerodynamic load distribution is part of the set of possible load distributions, very unrealistic perturbations will also be included. When incorporated in a robust flutter analysis, this will lead to an excessively conservative worst-case flutter boundary. On the other hand, if the true uncertainty mechanism is not part of the uncertainty description the worst-case flutter boundary has no meaning at all. Further, any aerodynamic model of a real aircraft would in this case require a very large number of uncertainties, making the robust flutter analysis too computationally expensive.

The key to the development of useful uncertainty descriptions is to bound the true uncertainty mechanism as closely as possible, using a minimum number of uncertain degrees of freedom to achieve this. It is clear that any knowledge about the likely uncertainty mechanism is of great value, and in many cases physical insight can provide directions. For example, modeling of external store, wing tip, and control surface aerodynamics is likely to be associated with uncertainty. In such cases it would be desirable to confine the aerodynamic uncertainty to certain regions of the lifting surface (such as the wing tip) and, if appropriate, assume that the load distribution in each region is perturbed in a rather uniform manner.

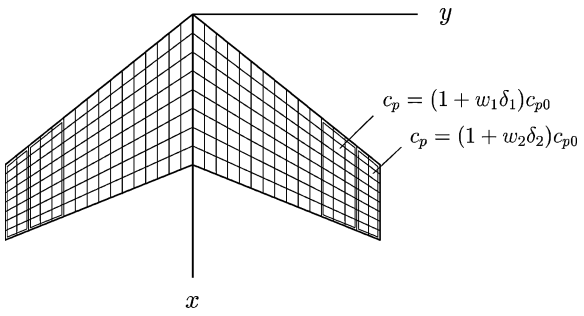

Fig. 1 Lifting surface with uncertain wing-tip loading; c_p denotes the uncertain pressure coefficients and c_{p0} the nominal values.

An uncertainty description that can achieve this is obtained by assigning the same uncertainty to a set of pressure coefficients, typically representing a certain region of the lifting surface. If panel method aerodynamics is used,[10–13] the panels can be divided into different patches with associated uncertainties δ_j. This is illustrated in Fig. 1 for a generic lifting surface with an uncertain spanwise lift distribution in the wing-tip region. Note that a different weight w_j can be used for each panel within a patch, such that the corresponding load distribution is perturbed uniformly but with different magnitude. However, such detailed information is rarely available, and the more simple model with one weight for each patch appears to be more useful. Using several patches will allow for models taking perturbations of the magnitude, phase shift, as well as distribution of the aerodynamic loading into account.

Note that the uncertain aerodynamic matrix for a model taking n uncertain patches (or regions) into account still can be written in the form Eq. (6). The only difference is that the matrices $\boldsymbol{E}_j$ in Eq. (5) now have unit entries at the diagonal elements corresponding to the panels being part of the jth patch.

The parametric uncertainty description Eq. (6) can be put in the more general form

$$\boldsymbol{Q}(ik, M) = \boldsymbol{Q}_0(ik, M) + \boldsymbol{V}_Q(ik, M)\boldsymbol{\Delta}_Q\boldsymbol{W}_Q \tag{7}$$

where in this case

$$\boldsymbol{V}_Q = [\boldsymbol{Q}_1 \quad \boldsymbol{Q}_2 \quad \cdots \quad \boldsymbol{Q}_n] \tag{8}$$

$$\boldsymbol{\Delta}_Q = \text{diag}(\delta_1\boldsymbol{I}_{m\times m}, \delta_2\boldsymbol{I}_{m\times m}, \ldots, \delta_n\boldsymbol{I}_{m\times m}) \tag{9}$$

$$\boldsymbol{W}_Q = \begin{bmatrix} w_1\boldsymbol{I}_{m\times m} \\ w_2\boldsymbol{I}_{m\times m} \\ \vdots \\ w_n\boldsymbol{I}_{m\times m} \end{bmatrix} \tag{10}$$

Hence, the uncertainty matrix $\boldsymbol{\Delta}_Q$ is diagonal $(n \times m) \times (n \times m)$ because each of the n parameters δ_j is repeated m times along the diagonal. In general, each parameter δ_j only needs to be repeated as many times as the rank of $\boldsymbol{Q}_j(ik, M)$ (Ref. 15). A rank-deficient matrix $\boldsymbol{Q}_j(ik, M)$ means that there exist nonzero deformations $\boldsymbol{\eta}$ for which the aerodynamic loads on the corresponding patch vanish. Typically, small patches or a large number of modes will lead to rank-deficient matrices $\boldsymbol{Q}_j(ik, M)$, and it might be necessary to compute an equivalent reduced-size structure.[16] However, if it is not obvious that most of the matrices $\boldsymbol{Q}_j(ik, M)$ have low rank the structure in Eqs. (8–10) is convenient to use. Now, in the more general form Eq. (7) the magnitude of the uncertainty is determined by the weighting matrix $\boldsymbol{W}_Q$ such that $\|\boldsymbol{\Delta}_Q\|_\infty \leq 1$, and the perturbation matrix $\boldsymbol{V}_Q(ik, M)$ determines the influence of the uncertain parameters on the aerodynamics.

The most simple uncertainty descriptions considered in this paper can be obtained directly from $\boldsymbol{Q}_0(ik, M)$. A model with an uncertain aerodynamic modal participation is defined by the simple structure

$$\boldsymbol{V}_Q = \boldsymbol{Q}_0 \tag{11}$$

$$\boldsymbol{\Delta}_Q = \text{diag}(\delta_1, \delta_2, \ldots, \delta_m) \tag{12}$$

$$\boldsymbol{W}_Q = \text{diag}(w_1, w_2, \ldots, w_m) \tag{13}$$

Note that this corresponds to a model with one full configuration patch for each mode. A 10% uncertainty in the contribution from the first mode is obtained by setting $w_1 = 0.1$. Note that $\boldsymbol{\Delta}_Q$ is only $m \times m$ because the perturbation matrices $\boldsymbol{Q}_j(ik, M)$ in the expansion Eq. (6) only have rank 1.

A less constrained model is obtained by assigning uncertainty to the aerodynamic influence coefficients (AICs). If $\boldsymbol{q}_{0j}$ denotes the jth column in $\boldsymbol{Q}_0(ik, M)$ and $\boldsymbol{I}_{m\times 1}$ an $m \times 1$ vector with unit entries, the following structure applies:

$$\boldsymbol{V}_Q = [\text{diag}(\boldsymbol{q}_{01}) \quad \text{diag}(\boldsymbol{q}_{02}) \quad \cdots \quad \text{diag}(\boldsymbol{q}_{0m})] \tag{14}$$

$$\boldsymbol{\Delta}_Q = \text{diag}(\delta_{11}, \delta_{12}, \ldots, \delta_{\text{mm}}) \tag{15}$$

$$\boldsymbol{W}_Q = \begin{bmatrix} [w_{11}\boldsymbol{I}_{m\times 1} & 0 & 0 & \cdots & 0] \\ [0 & w_{12}\boldsymbol{I}_{m\times 1} & 0 & \cdots & 0] \\ & & \vdots & & \\ [0 & 0 & \cdots & 0 & w_{\text{mm}}\boldsymbol{I}_{m\times 1}] \end{bmatrix} \tag{16}$$

A weight $w_{11} = 0.1$ means that a 10% uncertainty is assigned to the first diagonal element of $\boldsymbol{Q}_0(ik, M)$. In this case, $\boldsymbol{\Delta}_Q$ is $(m \times m) \times (m \times m)$.

It is clear that the developed uncertainty description benefits from the same level of geometric detail as the underlying aerodynamic model. Another important feature is that the uncertainty can be restricted to specific modes. For example, this can be utilized for modeling of uncertainty in control surface aerodynamics only, which will be demonstrated in the subsequent case study. Further, the influence from different patches (perhaps representing different uncertainty mechanisms) can be superposed, both in an additive and multiplicative manner. Moreover, an uncertainty description with an arbitrary number of uncertain patches, influencing only certain modes and so on, can be computed by simple postprocessing of standard aerodynamic data. The only requirement is that the decomposed form Eq. (3) of the nominal aerodynamic matrix is available. Next, a frequency-domain method for robust flutter analysis, which is capable of incorporating the developed uncertainty descriptions, will be outlined.

The μ-k Method for Robust Flutter Solutions

Now consider the case when all transfer functions in Eq. (1) are subject to parametric uncertainty,

$$\boldsymbol{M} = \boldsymbol{M}_0 + \boldsymbol{V}_M\boldsymbol{\Delta}_M\boldsymbol{W}_M \tag{17}$$

$$\boldsymbol{D} = \boldsymbol{D}_0 + \boldsymbol{V}_D\boldsymbol{\Delta}_D\boldsymbol{W}_D \tag{18}$$

$$\boldsymbol{K} = \boldsymbol{K}_0 + \boldsymbol{V}_K\boldsymbol{\Delta}_K\boldsymbol{W}_K \tag{19}$$

$$\boldsymbol{Q}(p, M) = \boldsymbol{Q}_0(p, M) + \boldsymbol{V}_Q(p, M)\boldsymbol{\Delta}_Q\boldsymbol{W}_Q \tag{20}$$

where the notation follows that in the preceding section. The essential differences are that the parametric perturbations to the mass, structural modal damping and stiffness matrices are real valued and do not depend on the flight condition. The uncertain parameters are scaled such that all uncertainty matrices have a norm less than unity.

Flutter Loop

To use structured singular value analysis[15,17] for robust flutter analysis, the uncertain flutter equation obtained by introducing Eqs. (17–20) in Eq. (1) is posed as the feedback loop in Fig. 2. This is accomplished by introducing the total uncertainty matrix

$$\boldsymbol{\Delta} = \text{diag}(\boldsymbol{\Delta}_M, \boldsymbol{\Delta}_D, \boldsymbol{\Delta}_K, \boldsymbol{\Delta}_Q) \tag{21}$$

the input signals z to the uncertainty matrix

$$z = \boldsymbol{W}\boldsymbol{\eta} \tag{22}$$

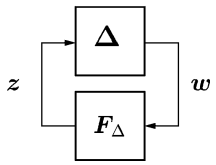

Fig. 2 Feedback loop representation of the uncertain flutter equation; the flutter loop.

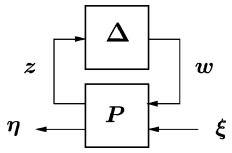

Fig. 3 LFT representation of the uncertain input-output system.

where the total weighting matrix

$$\boldsymbol{W} = \begin{bmatrix} \boldsymbol{W}_M \\ \boldsymbol{W}_D \\ \boldsymbol{W}_K \\ \boldsymbol{W}_Q \end{bmatrix} \tag{23}$$

and the output signals from the uncertainty matrix

$$w = \boldsymbol{\Delta}z \tag{24}$$

The influence of the uncertain output signals can now be separated from the nominal dynamics in the uncertain flutter equation, which in a compact form reads

$$\boldsymbol{F}_0(p, q, M)\boldsymbol{\eta} = \boldsymbol{V}(p, q, M)\boldsymbol{w} \tag{25}$$

where

$$\boldsymbol{F}_0(p, q, M) = \left[\boldsymbol{M}_0p^2 + (L/V)\boldsymbol{D}_0p + (L^2/V^2)\boldsymbol{K}_0 - (\rho L^2/2)\boldsymbol{Q}_0(p, M)\right] \tag{26}$$

is recognized as the nominal flutter transfer function matrix and

$$\boldsymbol{V}(p, q, M) = \left[-\boldsymbol{V}_Mp^2 \quad -(L/V)\boldsymbol{V}_Dp \quad -(L^2/V^2)\boldsymbol{V}_K \quad (\rho L^2/2)\boldsymbol{V}_Q(p, M)\right] \tag{27}$$

is the total perturbation transfer function matrix. The flutter loop transfer function matrix $\boldsymbol{F}(p, q, M)$ relates the signals $\boldsymbol{w}$ and z, and Eqs. (22) and (25) provide the convenient result

$$\boldsymbol{F}(p, q, M) = \boldsymbol{W}\boldsymbol{F}_0^{-1}(p, q, M)\boldsymbol{V}(p, q, M) \tag{28}$$

Note that $\boldsymbol{F}(p, q, M)$, which together with the structure of $\boldsymbol{\Delta}$ has the same importance to robust flutter analysis as does $\boldsymbol{F}_0(p, q, M)$ to nominal flutter analysis, is completely determined by $\boldsymbol{F}_0(p, q, M)$ and the uncertainty description Eqs. (17–20). Also note that the sign of each partition in $\boldsymbol{V}(p, q, M)$ can be chosen arbitrarily because if the system is stable subject to $\boldsymbol{\Delta}_M$ it is also stable subject to $-\boldsymbol{\Delta}_M$ and so on.

For a more general aeroelastic system involving control inputs and measured outputs, the flutter loop will constitute an inner loop of the uncertain system. In particular, the flutter loop can be isolated to the uncertain dynamics between the generalized force input $\boldsymbol{\xi}$ and the resulting generalized motion $\boldsymbol{\eta}$. Consider the present system with a generalized force input,

$$\boldsymbol{F}_0(p, q, M)\boldsymbol{\eta} = \boldsymbol{V}(p, q, M)\boldsymbol{w} + \boldsymbol{\xi} \tag{29}$$

The uncertain transfer function between the input $\boldsymbol{\xi}$ and the output $\boldsymbol{\eta}$ can be posed as the upper linear fractional transformation (LFT)[15] in Fig. 3, where the structure

$$\boldsymbol{P}(p, q, M) = \begin{bmatrix} \boldsymbol{P}_{11} & \boldsymbol{P}_{12} \\ \boldsymbol{P}_{21} & \boldsymbol{P}_{22} \end{bmatrix} = \begin{bmatrix} \boldsymbol{W}\boldsymbol{F}_0^{-1}\boldsymbol{V} & \boldsymbol{W}\boldsymbol{F}_0^{-1} \\ \boldsymbol{F}_0^{-1}\boldsymbol{V} & \boldsymbol{F}_0^{-1} \end{bmatrix} \tag{30}$$

is easily derived in the same manner as for the flutter loop. The uncertain transfer function matrix between $\boldsymbol{\xi}$ and $\boldsymbol{\eta}$ is now given by the upper LFT

$$\boldsymbol{\eta} = \mathcal{F}_u(\boldsymbol{P}, \boldsymbol{\Delta})\boldsymbol{\xi} = \left[\boldsymbol{P}_{22} + \boldsymbol{P}_{21}\boldsymbol{\Delta}(\boldsymbol{I} - \boldsymbol{P}_{11}\boldsymbol{\Delta})^{-1}\boldsymbol{P}_{12}\right]\boldsymbol{\xi} \tag{31}$$

If the system is nominally stable, the only source of instability is the term $(\boldsymbol{I} - \boldsymbol{P}_{11}\boldsymbol{\Delta})^{-1}$, which is equivalent to stability of an isolated $\boldsymbol{P}_{11}$-$\boldsymbol{\Delta}$ loop.[17] Further, the partition $\boldsymbol{P}_{11}$ is identified as the flutter loop transfer function matrix $\boldsymbol{F} = \boldsymbol{W}\boldsymbol{F}_0^{-1}\boldsymbol{V}$ in Eq. (28). Stability of the input-output system is thus equivalent to stability of the flutter loop.

In a more general setting, it is convenient to define the flutter loop transfer function matrix as

$$\boldsymbol{F}(p, q, M) = \boldsymbol{P}_{11}(p, q, M) \tag{32}$$

where $\boldsymbol{P}_{11}(p, q, M)$ is the corresponding partition of the upper LFT between the generalized force input $\boldsymbol{\xi}$ and the generalized coordinates $\boldsymbol{\eta}$. For example, the uncertainty description Eqs. (17–20) only considers a linear dependence on the uncertain parameters δ_j. If higher-order parametric perturbations or nonparametric uncertainty need to be considered,[18] the LFT framework from robust control[15] can be utilized to form the corresponding flutter loop. The LFT framework is also convenient for posing different subsystems as LFTs, which will be utilized in the subsequent case study.

The definition Eq. (32) is valid for aeroservoelastic systems as well, where the corresponding loop can include uncertain controller dynamics, sensor dynamics, actuator dynamics, control surface aerodynamics, and so on. In this case, the loop will represent the uncertain equations of motion for the transient dynamics of the aeroservoelastic system.

Robust Flutter Analysis and μ-k Graphs

Flutter stability of the uncertain aeroelastic system is now equivalent to stability of the flutter loop in Fig. 2, where the structured uncertainty set has been scaled such that $\|\boldsymbol{\Delta}\|_\infty \leq 1$. If the system is nominally stable at a particular flight condition (which is determined by the nominal flutter boundary), the system is also robustly stable subject to the specified uncertainty if the structured singular value[17]

$$\mu(k, q, M) = \mu[\boldsymbol{F}(ik, q, M)] < 1, \qquad \forall\, k \geq 0 \tag{33}$$

Note that the stability criterion Eq. (33) only sensors the frequency response of the uncertain system. Consequently, only the frequency-domain aerodynamic matrices $\boldsymbol{Q}_0(ik, M)$ and $\boldsymbol{V}_Q(ik, M)$ are required for the robust flutter analysis.

A worst-case match-point flutter boundary can now be computed in essentially the same manner as the nominal flutter boundary. The reduced frequency range of interest is discretized into a set k_j, $j = 1, \ldots, n_k$, of reduced frequencies. The dynamic pressure q is increased in successive steps while keeping Mach M fixed. For each dynamic pressure the structured singular values $\mu(k_j, q, M)$ are computed, and if all $\mu(k_j, q, M) < 1$ the system is robustly stable. The robust critical dynamic pressure is reached when any $\mu(k_j, q, M)$ crosses the stability boundary $\mu(k, q, M) = 1$. This procedure is repeated for each Mach M of interest, which provides a worst-case flutter boundary subject to the specified uncertainty.

Consider the scenario when an eigenvalue $p = g + ik$ of the nominal system approaches the flutter boundary $g = 0$ when q is increased at constant M. In the corresponding μ-k graphs, this will become visible as a distinct peak in the neighborhood of the reduced frequency of the eigenvalue. This is illustrated in Fig. 4 for four different values of the dynamic pressure q. The μ-k graphs in Fig. 4 actually represent the behavior of the wind-tunnel model in the subsequent case study, but are here used for illustration purposes only. In this case the peak of the μ-k graphs moves from the right to the left in the figure when q is increased (k of the nominal critical mode is reduced when q is increased). The right-most graph corresponds to a low q for which the system is robustly stable. When q is increased to q_{rob}, the μ-k graph touches the robust flutter boundary

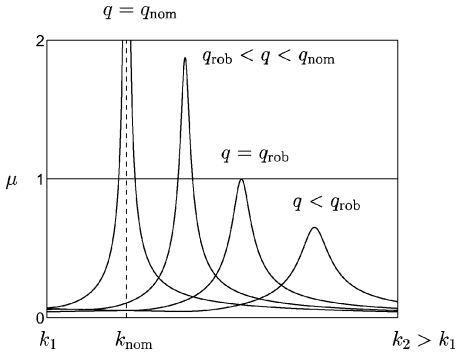

Fig. 4 Example μ-k graphs when q is increased at constant M. The solid horizontal line indicates the robust flutter boundary, and the dashed vertical line indicates the nominal reduced flutter frequency.

$\mu(k, q, M) = 1$ and q_{rob} is the worst-case critical dynamic pressure at the considered value of M.

When q is increased further, the μ-k graph appears to approach a singularity. This is also the case because $1/\mu(k, q, M)$ is defined as the minimum norm of $\boldsymbol{\Delta}$ (at the reduced frequency k) for which there exist some structured $\boldsymbol{\Delta}$ that destabilize the loop in Fig. 2 (Ref. 17). When the eigenvalue p approaches the nominal stability boundary $g = 0$, it is clear that the norm of $\boldsymbol{\Delta}$ required for this tends to zero, and $\mu(k, q, M)$ will display a singularity at the nominal flutter frequency $k = k_{\text{nom}}$ when the nominal flutter boundary $q = q_{\text{nom}}$ is reached (see Fig. 4). Also note that the inverse $\boldsymbol{F}_0^{-1}(ik, q, M)$ does not exist at the nominal flutter boundary because the nominal flutter matrix $\boldsymbol{F}_0(ik, q, M)$ is singular at this condition.

In this and previous work on robust aeroservoelastic analysis, it is assumed that the standard μ framework can be applied. Although this is a reasonable assumption in practice, the aerodynamic transfer function matrix $\boldsymbol{Q}(p, M)$ in Eq. (1) has a nonrational dependence on p (Ref. 19), whereas the standard μ framework applies to systems represented by rational transfer function matrices. Computing μ involves the solution of an optimization problem, which is nonpolynomial hard,[20] and much effort has been devoted to derive upper and lower bounds tight enough for practical applications. In particular, computing bounds on μ for purely real uncertainty sets has proved difficult.[14] However, if some amount of aerodynamic uncertainty (which is always present in practice) is considered in the robust flutter analysis a complex or mixed real/complex (aerodynamic or mixed structural/aerodynamic uncertainty) μ problem will result, for which solvers are available in established software packages.[21]

So far it has been assumed that the structure as well as the magnitude of the uncertainty are given. Although the development of the structure (in particular for the aerodynamics) has been discussed in some detail, how to estimate the magnitude has not. In the case of flight testing of a new aircraft configuration, this step is vital if the testing should be supported by a useful robust flutter boundary.[22,23] However, a possible application of robust analysis might also be efficient identification of likely reasons for flutter mechanisms encountered later on in a flight program, such as limit-cycle oscillations.[24] Nevertheless, if suitable experimental data are available (or acquired during flight testing) the μ framework allows for an estimation of the model uncertainty bound.[7] In this paper, this procedure will be given some attention in connection to the application that follows in the next section.

Application to a Wind-Tunnel Model

The wind-tunnel experiment in Borglund[5] and Borglund and Nilsson[6] is revisited. As shown in Fig. 5, a flexible wing with a controllable trailing-edge flap is mounted in a low-speed wind tunnel at the Royal Institute of Technology. An optical measurement system is used to monitor the elastic deflection y at a midspan leading-edge position on the wing. In this study, a MATLAB® numerical analysis based on beam finite element structural analysis and doublet-lattice aerodynamics[10,11] is used. However, only the main planform of the wing is part of the aerodynamic model, and the influence from the

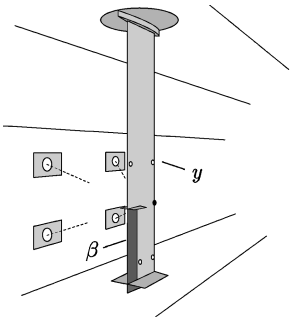

Fig. 5 Schematic of the wind-tunnel model showing the flap deflection β, the measured wing deflection y, and the wing-tip vertical plate.

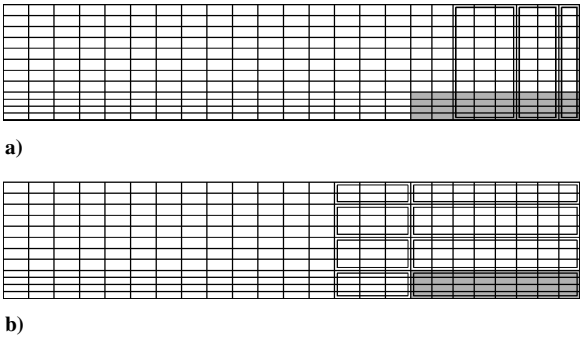

Fig. 6 Panel geometry and uncertain patches for the wind-tunnel model: a) the spanwise wing-tip patches applies to all modes and b) the chordwise patches only to the flap mode.

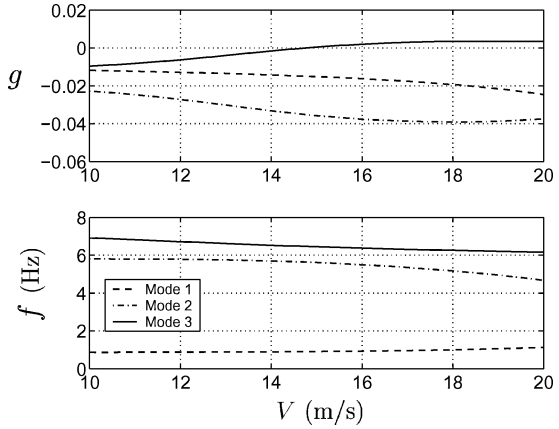

Fig. 7 *V-g* and *V-f* diagrams of the wind-tunnel model: three modes.

vertical plate and actuator compartment located at the wing tip is neglected (see Fig. 6). Further, the μ toolbox[21] in MATLAB® is utilized for the subsequent μ computations.

Nominal Flutter Analysis

In this problem the flap aerodynamics is only part of a forcing term in the nominal Laplace-domain equations of motion,

$$\boldsymbol{F}_0(p, V)\boldsymbol{\eta}(p) = \left[\boldsymbol{b}_0 p^2 + (\rho L^2/2)\boldsymbol{q}_0(p, V)\right]\beta(p) = \boldsymbol{f}_0(p, V)\beta(p) \tag{34}$$

$$y(p) = \boldsymbol{c}_0^T \boldsymbol{\eta}(p) \tag{35}$$

where $\boldsymbol{F}_0(p, V)$ is defined in Eq. (26) and $\boldsymbol{b}_0$ and $\boldsymbol{q}_0(p, V)$ determines the inertial and aerodynamic forces caused by flap motion, respectively ($M = 0.0$ because of the low-speed conditions). Further, the measured wing deflection $y(p)$ is related to the generalized coordinates $\boldsymbol{\eta}(p)$ through the generalized output matrix $\boldsymbol{c}_0^T$.

A standard p-k flutter analysis reveals that using only $m = 3$ modes provides an accurate nominal analysis, and the corresponding V-g and V-f diagrams are shown in Fig. 7. The wing is predicted to flutter in the third mode at the nominal flutter speed $V_{\text{nom}} = 14.7$ m/s with a flutter frequency $f_{\text{nom}} = 6.5$ Hz. Further, the frequency-response-function (FRF) data between the flap deflection β and the measured deflection y at the midwing leading-edge position are available for $V = 10$ m/s in the frequency range of interest. These data are displayed in Fig. 8 along with a nominal prediction of the response. Although the prediction of the phase shift agrees quite well with the experimental data, a larger discrepancy is observed for the magnitude. The problem posed is to perform a robust flutter analysis based on the available data.

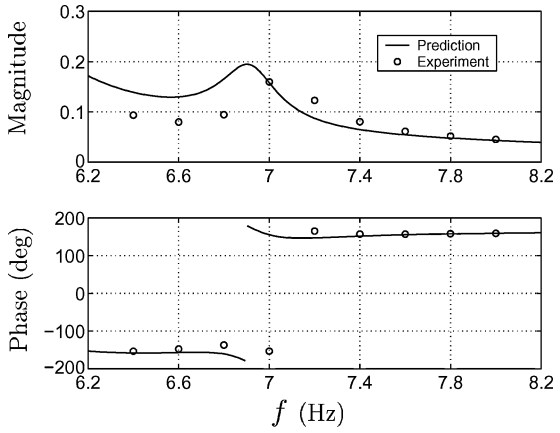

Fig. 8 Bode diagram of the frequency response between β (rad) and y (fraction semichord) at $V = 10$ m/s.

Modeling of Aerodynamic Uncertainty

The accuracy of the structural analysis is quite remarkable for the present problem,[25] and it is reasonable to assume that the neglected wing-tip aerodynamics is the dominant uncertainty that can affect the flutter behavior. An uncertain spanwise lift distribution in the wing-tip region is therefore assumed for all modes, including the flap aerodynamics, and three uncertain patches are introduced for this purpose (see Fig. 6a). In addition to this, the flap mode aerodynamics is assumed to have an uncertain chordwise lift distribution. Eight patches are introduced to represent this (see Fig. 6b). The four inboard patches are separate from the four outboard patches in order to model the likely uncertainty in the region close to the inboard flap edge, where a small vertical plate is also located (see Fig. 5). For simplicity, the same weight w_Q is assigned to the three wing-tip patches, and the same weight w_q is assigned to the eight flap mode patches.

Fourteen aerodynamic perturbation matrices need to be computed based on this structure of the aerodynamic uncertainty, three matrices $\boldsymbol{Q}_j(ik)$ for the influence from the wing-tip patches on the wing load distribution and 11 vectors $\boldsymbol{q}_j(ik)$ for the influence from all patches on the flap load distribution. The uncertain aerodynamic matrix can be written as

$$\boldsymbol{Q}(ik) = \boldsymbol{Q}_0(ik) + \sum_{j=1}^{3} \delta_j w_j \boldsymbol{Q}_j(ik) = \boldsymbol{Q}_0(ik) + \boldsymbol{V}_Q(ik)\boldsymbol{\Delta}_Q \boldsymbol{W}_Q \tag{36}$$

where in this case

$$\boldsymbol{V}_Q = [\boldsymbol{Q}_1 \quad \boldsymbol{Q}_2 \quad \boldsymbol{Q}_3] \tag{37}$$

$$\boldsymbol{\Delta}_Q = \text{diag}(\delta_1 \boldsymbol{I}_{3\times 3}, \delta_2 \boldsymbol{I}_{3\times 3}, \delta_3 \boldsymbol{I}_{3\times 3}) \tag{38}$$

$$\boldsymbol{W}_Q = \begin{bmatrix} w_Q \boldsymbol{I}_{3\times 3} \\ w_Q \boldsymbol{I}_{3\times 3} \\ w_Q \boldsymbol{I}_{3\times 3} \end{bmatrix} \tag{39}$$

In the same manner the uncertain aerodynamic vector for the flap aerodynamics is

$$\boldsymbol{q}(ik) = \boldsymbol{q}_0(ik) + \sum_{j=1}^{11} \delta_j w_j \boldsymbol{q}_j(ik) = \boldsymbol{q}_0(ik) + \boldsymbol{V}_q(ik)\boldsymbol{\Delta}_q \boldsymbol{W}_q \tag{40}$$

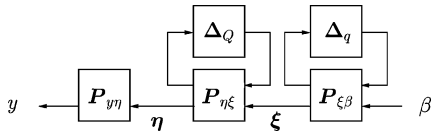

Fig. 9 Uncertain aeroelastic system as a combination of LFT subsystems.

where

$$\boldsymbol{V}_q = [\boldsymbol{q}_1 \quad \boldsymbol{q}_2 \quad \cdots \quad \boldsymbol{q}_{11}] \tag{41}$$

$$\boldsymbol{\Delta}_q = \mathrm{diag}(\delta_1, \delta_2, \ldots, \delta_{11}) \tag{42}$$

$$\boldsymbol{W}_q = \begin{bmatrix} w_Q \\ w_Q \\ w_Q \\ w_q \\ \vdots \\ w_q \end{bmatrix} \tag{43}$$

which completes the structure of the uncertainty description. The uncertain aeroelastic system between $\beta(p)$ and $y(p)$ can now be represented by the LFT interconnection in Fig. 9, where the subsystems

$$\boldsymbol{P}_{\xi\beta} = \begin{bmatrix} 0 & \boldsymbol{W}_q \\ (\rho L^2/2)\boldsymbol{V}_q & \boldsymbol{f}_0 \end{bmatrix} \tag{44}$$

$$\boldsymbol{P}_{\eta\xi} = \begin{bmatrix} (\rho L^2/2)\boldsymbol{W}_Q\boldsymbol{F}_0^{-1}\boldsymbol{V}_Q & \boldsymbol{W}_Q\boldsymbol{F}_0^{-1} \\ (\rho L^2/2)\boldsymbol{F}_0^{-1}\boldsymbol{V}_Q & \boldsymbol{F}_0^{-1} \end{bmatrix} \tag{45}$$

$$\boldsymbol{P}_{y\eta} = \boldsymbol{c}_0^T \tag{46}$$

Note that the uncertainty $\boldsymbol{\Delta}_q$ associated with the input does not influence the dynamics in a feedback manner, and the only source of instability is the flutter loop in the LFT $\mathcal{F}_u(\boldsymbol{P}_{\eta\xi}, \boldsymbol{\Delta}_Q)$. Next, the magnitude of the uncertainty present in the model will be estimated.

Model Validation

In this study the uncertainty in the flap aerodynamics has to be included because it influences the frequency response between $\beta(p)$ and $y(p)$ to be used for validation of the model (recall Fig. 8). To use the approach by Kumar and Balas[7] for model validation, the uncertain system between $\beta(p)$ and $y(p)$ is posed as a single upper LFT. An interconnection of LFTs is also an LFT,[15] and for the present problem it is a straightforward matter to show that $\mathcal{F}_u(\boldsymbol{P}, \boldsymbol{\Delta})$, where

$$\boldsymbol{P} = \left[\begin{array}{cc|c} (\rho L^2/2)\boldsymbol{W}_Q\boldsymbol{F}_0^{-1}\boldsymbol{V}_Q & (\rho L^2/2)\boldsymbol{W}_Q\boldsymbol{F}_0^{-1}\boldsymbol{V}_q & \boldsymbol{W}_Q\boldsymbol{F}_0^{-1}\boldsymbol{f}_0 \\ 0 & 0 & \boldsymbol{W}_q \\ \hline (\rho L^2/2)\boldsymbol{c}_0^T\boldsymbol{F}_0^{-1}\boldsymbol{V}_Q & (\rho L^2/2)\boldsymbol{c}_0^T\boldsymbol{F}_0^{-1}\boldsymbol{V}_q & \boldsymbol{c}_0^T\boldsymbol{F}_0^{-1}\boldsymbol{f}_0 \end{array}\right] \tag{47}$$

$$\boldsymbol{\Delta} = \mathrm{diag}(\boldsymbol{\Delta}_Q, \boldsymbol{\Delta}_q) \tag{48}$$

represents the uncertain system between $\beta(p)$ and $y(p)$. In particular, the partition $P_{22} = \boldsymbol{c}_0^T\boldsymbol{F}_0^{-1}\boldsymbol{f}_0$ is recognized as the nominal transfer function between $\beta(p)$ and $y(p)$.

Now consider the FRF data in Fig. 8. For each experimental frequency k_j there is an experimental value $P_{22}^{\exp}(k_j, V)$ and a corresponding nominal prediction $P_{22}(ik_j, V)$. As shown in Kumar and Balas,[7] the uncertain system with $\|\boldsymbol{\Delta}\|_\infty \le 1$ can match the experimental data if all of the structured singular values

$$\mu_{\mathrm{val}}(k_j, V) = \mu\left[\boldsymbol{P}_{11} - \boldsymbol{P}_{12}\left(P_{22} - P_{22}^{\exp}\right)^{-1}\boldsymbol{P}_{21}\right] > 1 \tag{49}$$

Table 1 Estimated magnitude of the uncertainty based on model validation at $V = 10$ m/s

Model	δ_j (no.)	$\boldsymbol{\Delta}$ (size)	w_q/w_Q	w_Q	w_q
AIC	12	12×12	2	0.14	0.28
Modal	4	4×4	2	0.16	0.33
Detailed	11	20×20	1	0.20	0.20

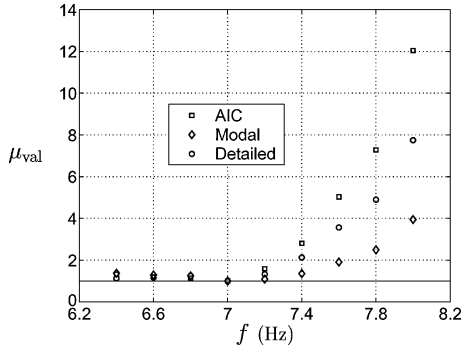

Fig. 10 Model validation at $V = 10$ m/s for the three different uncertainty descriptions.

Hence, the minimum magnitude of the uncertainty required to validate the experimental data can be computed by scaling the weights w_Q and w_q uniformly such that the minimum $\mu_{\mathrm{val}}(k_j, V) = 1$, which is very desirable in order not to make the subsequent robust flutter analysis more conservative than necessary.

Prior to the model validation, the ratio w_q/w_Q has to be specified. Unfortunately, it is not possible to determine this ratio based on the FRF data in Fig. 8, and an assumption about this has to be made in this study. For the present uncertainty description, it is therefore assumed that the magnitude of the chordwise uncertainty in the flap load distribution is equal to the magnitude of the spanwise uncertainty in the wing-tip region. This means that $w_q/w_Q = 1$ and that the load distribution caused by flap motion can be twice as uncertain in the wing-tip region compared to the inboard region where only chordwise uncertainty is considered.

The detailed uncertainty description will be compared to the more simple uncertainty representations considering uncertainty in the AICs and aerodynamic modal participation. The simple models are not detailed for this problem, but are simply represented by different matrices in Eqs. (37–39) and Eqs. (41–43). In these models, however, the knowledge about the likely uncertainty mechanism is not exploited at all. Each mode (or AIC) is assigned an individual uncertainty δ_j and the flap aerodynamics is assumed to be twice as uncertain as the wing aerodynamics ($w_q/w_Q = 2$ is used).

The result of the model validation for the three different models is presented in Fig. 10 and Table 1, respectively. All models require the largest magnitude of the uncertainty at the $f = 7.0$ Hz data point. At this frequency the error in the phase shift is the largest in the FRF data in Fig. 8. As expected, the model with uncertain AICs requires the least uncertainty to validate the experimental data, 14% for the wing aerodynamics and 28% for the flap aerodynamics. The model based on modal uncertainty requires slightly higher values, 16 and 33%, respectively. Finally, the detailed uncertainty description requires a 20% spanwise wing-tip uncertainty and a 20% chordwise flap uncertainty.

In general, the uncertainty bound can be allowed to vary across frequency.[7] However, care should be taken because the system dynamics change with the flight condition, and a tailored uncertainty description might not be fully representative at a different flight condition. In this study, the different models are simply validated in a worst-case manner in the frequency range of the critical flutter mode (recall Fig. 10). Uncertainty in the experimental data has to be considered in a more realistic setting, and advanced methods for processing of flight-test data for robust flutter analysis are continuously being improved.[18,26–28] In a flight-testing program, the estimation of the uncertainty bound would be followed by a robust

Table 2 Comparison between predicted and experimental results

Model	δ_j (no.)	Δ_Q (size)	V_{nom}, m/s	V_{rob}, m/s	$(V_{\text{nom}} - V_{\text{rob}})/V_{\text{nom}}$, %	V_{exp}, m/s
AIC	9	9×9	14.7	10.8	27	16.0
Modal	3	3×3	14.7	11.4	22	16.0
Detailed	3	9×9	14.7	13.3	10	16.0

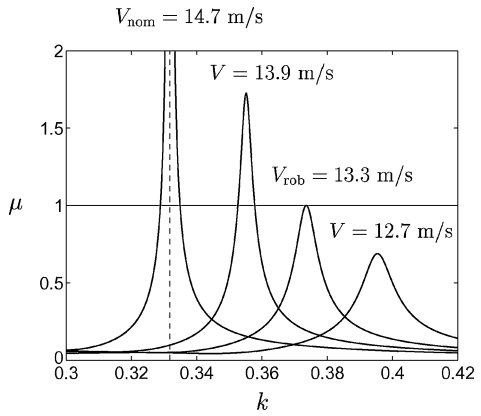

Fig. 11 μ-k graphs for the wind-tunnel model: detailed uncertainty description.

flutter prediction and a possible extension of the flight envelope,[22,23] which is also the next step in the present case study.

Robust Flutter Analysis

Robust stability is determined by the flutter loop, and the wing is robustly stable subject to the aerodynamic uncertainty specified in Eq. (36) if $V < V_{\text{nom}}$ and

$$\mu(k, V) = \mu[\boldsymbol{F}(ik, V)] = \mu\left[(\rho L^2/2)\boldsymbol{W}_Q \boldsymbol{F}_0^{-1} \boldsymbol{V}_Q\right] < 1 \quad \forall\, k \geq 0 \qquad (50)$$

The robust flutter speeds for the three different uncertainty descriptions are presented in Table 2. The model based on uncertain AICs is the most conservative, the model with modal uncertainty is somewhat less conservative, while the model based on the detailed uncertainty description is the least conservative and predicts a robust flutter speed 10% below the nominal value. The μ-k graphs for the detailed case are shown in Fig. 11. Also note that a detailed uncertainty description does not imply a large size uncertainty description, but rather that the likely uncertainty mechanism can be isolated.

In the experiment, the wing is found to flutter at $V_{\text{exp}} = 16.0$ m/s with a flutter frequency $f_{\text{exp}} = 6.4$ Hz. In fact, the influence of the wing-tip vertical plate stabilizes the critical mode in the experiment.[5] If it is assumed that the aerodynamic uncertainty can also increase the flutter speed by 10%, the maximum critical speed $V = 16.1$ m/s results. In this perspective, the detailed uncertainty description appears to result in a robust flutter analysis with a minimum level of conservatism. However, considering the complexity of the treated problem and that the weighting between the wing and flap aerodynamic uncertainty has not been determined experimentally, this observation is questionable. Nevertheless, the present case study has clearly indicated that a detailed aerodynamic uncertainty description can improve the robust flutter prediction.

Conclusions

The present work has provided two main contributions. First, a versatile uncertainty description for unsteady aerodynamic forces was derived by assigning uncertainty to the frequency-domain pressure coefficients. The uncertainty description applies to any frequency-domain aerodynamic method, benefits from the same level of geometric detail as the underlying aerodynamic model, can be restricted to specific modes, allows for superposition of different uncertainties, and is computed by simple postprocessing of standard aerodynamic data. Second, a straightforward frequency-domain method for robust flutter analysis was provided. With the present method, each flight condition is represented by a μ-k graph, which by continuation is used to determine the robust flutter boundary and the critical flutter mode. The μ-k procedure resembles a p-k or g-method flutter analysis, does not involve finite-state approximations of the aerodynamic forces, allows for detailed aerodynamic uncertainty descriptions, treats the uncertainty in the inertial, damping, elastic, and aerodynamic forces in a consistent manner, inherently produces match-point flutter solutions, applies to aeroservoelastic systems, and naturally results in a mixed real/complex μ problem if aerodynamic uncertainty is considered. Finally, a case study clearly indicated that the present method can improve the robust flutter prediction substantially in cases where a detailed aerodynamic uncertainty description can be developed.

Acknowledgments

The author is grateful to Ulf Ringertz who provided the implementation of the doublet-lattice method, and Sven Hedman for a fruitful discussion on panel method aerodynamics. This work was financially supported by The National Program for Aeronautics Research.

References

[1]Lind, R., and Brenner, M., *Robust Aeroservoelastic Stability Analysis*, Springer-Verlag, London, 1999.

[2]Lind, R., "Match-Point Solutions for Robust Flutter Analysis," *Journal of Aircraft*, Vol. 39, No. 1, 2002, pp. 91–99.

[3]Moulin, B., Idan, M., and Karpel, M., "Aeroservoelastic Structural and Control Optimization Using Robust Design Schemes," *Journal of Guidance, Control, and Dynamics*, Vol. 25, No. 1, 2002, pp. 152–159.

[4]Karpel, M., Moulin, B., and Idan, M., "Robust Aeroservoelastic Design with Structural Variations and Modeling Uncertainties," *Journal of Aircraft*, Vol. 40, No. 5, 2003, pp. 946–954.

[5]Borglund, D., "Robust Aeroelastic Stability Analysis Considering Frequency-Domain Aerodynamic Uncertainty," *Journal of Aircraft*, Vol. 40, No. 1, 2003, pp. 189–193.

[6]Borglund, D., and Nilsson, U., "Robust Wing Flutter Suppression Considering Frequency-Domain Aerodynamic Uncertainty," *Journal of Aircraft* (to be published).

[7]Kumar, A., and Balas, G. J., "An Approach to Model Validation in the μ Framework," *Proceedings of the American Control Conference*, Baltimore, MD, 1994, pp. 3021–3026.

[8]Bäck, P., and Ringertz, U. T., "On the Convergence of Methods for Nonlinear Eigenvalue Problems," *AIAA Journal*, Vol. 35, No. 6, 1997, pp. 1084–1087.

[9]Chen, P. C., "Damping Perturbation Method for Flutter Solution: The g-Method," *AIAA Journal*, Vol. 38, No. 9, 2000, pp. 1519–1524.

[10]Albano, E., and Rodden, W. P.,"A Doublet-Lattice Method for Calculating Lift Distributions on Oscillating Surfaces in Subsonic Flows," *AIAA Journal*, Vol. 7, No. 2, 1969, pp. 279–285.

[11]Rodden, W. P., Taylor, P. F., and McIntosh, S. C., Jr., "Further Refinement of the Nonplanar Aspects of the Subsonic Doublet-Lattice Lifting Surface Method," *Journal of Aircraft*, Vol. 35, No. 5, 1998, pp. 720–727.

[12]Chen, P. C., and Liu, D. D., "Unsteady Supersonic Computations of Arbitrary Wing-Body Configurations Including External Stores," *Journal of Aircraft*, Vol. 27, No. 2, 1990, pp. 108–116.

[13]Chen, P. C., and Liu, D. D., "Unsteady Subsonic Aerodynamics for Bodies and Wings with External Stores Including Wake Effect," *Journal of Aircraft*, Vol. 30, No. 5, 1993, pp. 618–628.

[14]Hayes, M. J., Bates, D. G., and Postlethwaite, I., "New Tools for Computing Tight Bounds on the Real Structured Singular Value," *Journal of Guidance, Control, and Dynamics*, Vol. 24, No. 6, 2001, pp. 1204–1213.

[15]Zhou, K., Doyle, J. C., and Glover, K., *Robust and Optimal Control*, Prentice–Hall, Upper Saddle River, N J, 1996, pp. 247–269.

[16]Cockburn, J. C., and Morton, B. G., "Linear Fractional Representations of Uncertain Systems," *Automatica*, Vol. 33, No. 7, 1997, pp. 1263–1271.

[17]Packard, A., and Doyle, J., "The Complex Structured Singular Value," *Automatica*, Vol. 29, No. 1, 1993, pp. 71–109.

[18]Brenner, M., "Aeroservoelastic Model Uncertainty Bound Estimation from Flight Data," *Journal of Guidance, Control, and Dynamics*, Vol. 25, No. 4, 2002, pp. 748–754.

[19]Stark, V. J., "General Equations of Motion for an Elastic Wing and Method of Solution," *AIAA Journal*, Vol. 22, No. 8, 1984, pp. 1146–1153.

[20]Braatz, R., Young, P., Doyle, J., and Morari, M., "Computational Complexity of μ Calculation," *IEEE Transactions on Automatic Control*, Vol. AC-39, No. 5, 1994, pp. 1000–1002.
[21]Balas, G. J., Doyle, J. C., Glover, K., Packard, A., and Smith, R., *μ-Analysis and Synthesis Toolbox User's Guide*, The MathWorks, Inc., Natick, MA, 1996, Chap. 4.
[22]Lind, R., and Brenner, M., "Flutterometer: An on-Line Tool to Predict Robust Flutter Margins," *Journal of Aircraft*, Vol. 37, No. 6, 2000, pp. 1105–1112.
[23]Lind, R., "Flight-Test Evaluation of Flutter Prediction Methods," *Journal of Aircraft*, Vol. 40, No. 5, 2003, pp. 964–970.
[24]Norton, W. J., "Limit Cycle Oscillations and Flight Testing," *Proceedings of the 21st Annual Symposium, Society of Flight Test Engineers*, Lancaster, CA, 1990, pp. 3.4.1–3.4.12.
[25]Borglund, D., and Kuttenkeuler, J., "Active Wing Flutter Suppression Using a Trailing Edge Flap," *Journal of Fluids and Structures*, Vol. 16, No. 3, 2002, pp. 271–294.
[26]Brenner, M., and Lind, R., "Wavelet-Processed Flight Data for Robust Aeroservoelastic Stability Margins," *Journal of Guidance, Control, and Dynamics*, Vol. 21, No.6, 1998, pp. 823–829.
[27]Johnson, J. D., Lu, J., Dhawan, A. P., and Lind, R., "Real-Time Identification of Flutter Boundaries Using the Discrete Wavelet Transform," *Journal of Guidance, Control, and Dynamics*, Vol. 25, No. 2, 2002, pp. 334–339.
[28]Prazenica, R. J., Lind, R., and Kurdila, A. J., "Uncertainty Estimation from Volterra Kernels for Robust Flutter Analysis," *Journal of Guidance, Control, and Dynamics*, Vol. 26, No. 2, 2003, pp. 331–339.